

Microstructural properties of hardened cement paste blended with coal fly ash, sugar mill lime sludge and rice hull ash

Einstine M. Opiso^{*1}, Tsutomu Sato^{2a} and Tsubasa Otake^{2b}

¹Department of Civil Engineering, College of Engineering, Central Mindanao University, Musuan, Bukidnon, 8710, Philippines

²Laboratory of Environmental Geology, Graduate School of Engineering, Hokkaido University, Sapporo, Japan

(Received February 13, 2017, Revised June 19, 2017, Accepted June 20, 2017)

Abstract. The synergistic interactions of supplementary cementitious materials (SCMs) with ordinary portland cement (OPC) in multi-blended systems could enhance the mechanical and durability properties of concrete and increase the amount of cement that can be replaced. In this study, the characteristics of the hydration products as well as paste microstructure of blended cement containing 20% coal fly ash, 10% rice hull ash and 10% sugar mill lime sludge in quaternary blended system was investigated. Portlandite content, hydration products, compressive strength, pore size distribution and microstructural architecture of hydrated blended cement pastes were examined. The quaternary blended cement paste showed lower compressive strength, reduced amount of Portlandite phases, and higher porosity compared to plain hardened cement paste. The interaction of SCMs with OPC influenced the hydration products, resulting to the formation of ettringite and monocarboaluminate phases. The blended cement paste also showed extensive calcium silicate hydrates and calcium aluminate silicate hydrates but unrefined compared to plain cement paste. In overall, the expected synergistic reaction was significantly hindered due to the low quality of supplementary cementitious materials used. Hence, pre-treatments of SCMs must be considered to enhance their reactivity as good quality SCMs can become limited in the future.

Keywords: quaternary blended cement; synergistic interactions; multi-blended systems; supplementary cementitious materials; coal fly ash; rice hull ash; sugar mill lime sludge

1. Introduction

The use of supplementary cementitious materials (SCMs) such as coal fly ash (CFA), limestone powder, steel slag, silica fume, meta-kaolin clay and biomass ashes in the production of cement and as partial replacement to cement in concrete has received considerable attention nowadays. This is because the utilization of SCMs could significantly lessen the environmental impact of cement and concrete production by providing alternative solution to the disposal problems of SCMs and by reducing CO₂ emissions (Juenger and Siddique 2015). Moreover, SCMs can

*Corresponding author, Assistant Professor, E-mail: einstineopiso@cmu.edu.ph

^aProfessor

^bAssociate Professor

improve the mechanical and durability properties of concrete (Nadeem *et al.* 2013, Ferraro and Nanni 2012). A study by Chore *et al.* (2015) showed that fly ash mixed with cement at 7.5% increases concrete strength up to 46.81 N/mm² at 7 days curing.

One of the focus researches recently is the interactions of SCMs with OPC in multi-blended systems. SCMs have synergistic interaction with OPC that results into the improvement of the mechanical and durability properties of concrete and thereby increasing the amount of cement that can be replaced (Juenger and Siddique 2015, Kathirvel *et al.* 2013). Recent studies on multi-blended systems which reported significant improvement in terms of strength and durability of cement mortar in ternary blended systems include OPC, rice hull ash (RHA) and CFA (Chindaprasirt and Rukson 2008); OPC, limestone filler and blast-furnace slag (Menendez *et al.* 2003); OPC, CFA and limestone powder (De Weerd *et al.* 2011); OPC, RHA, and Silpozz (Panda *et al.* 2015) and in quaternary blending of OPC, CFA, RHA and limestone powder (Kathirvel *et al.* 2013). Moreover, CFA is widely accepted to contribute in the improvement of strength development in the later stage since it will react slowly in the formation of calcium aluminate precipitates (De Weerd *et al.* 2011). The incorporation of CFA also produces filler and dispersing effects and increases the nucleation and precipitation sites (Chindaprasirt and Rukson 2008). Limestone powder, on the other hand, could offset the compromise of early strength development caused by CFA as it acts as nucleation site for CSH during the hydration of cement (De Weerd *et al.* 2011). Lastly, RHA also have filler effect due to its fine particle size (Chindaprasirt and Rukson 2008) and its pozzolanic action could result in the formation of more calcium silicate hydrates (CSH) gel (Kathirvel *et al.* 2013).

In Northern Mindanao, Philippines, among the SCMs that are widely available and posed huge potential in the development of eco-cement material include CFA from coal fired power plants, sugar mill lime sludge (SMLS) from sugar milling companies and RHA from the rice production areas. Recent studies revealed that up to 30-40% and 10-20% of OPC could be replaced by coal fly ash and lime powder, respectively, without any deleterious effect on the strength properties of concrete (De Weerd *et al.* 2011). Specifically, sugar mill lime sludge essentially contains lime as major constituent. In the case of RHA, there is a general consensus in the literature that RHA could be used up to 10-20% as partial replacement to cement (Ferraro and Nanni 2012, Madandoust *et al.* 2011, Chindaprasirt and Rukson 2008). However, studies investigating the strength and microstructural properties of hardened cement paste in quaternary blended systems are very limited particularly on the use of CFA, RHA and SMLS.

In this context, this paper aims to determine the compressive strength and microstructural properties of hardened cement paste blended with higher replacement percentage of SCMs. In this study, a 2:1:1 blending ratio of CFA, RHA and SMLS was employed based on the results from a recent study of Kathirvel *et al.* (2013). The quaternary blended hardened cement paste at different curing periods was tested for Ca(OH)₂ content, pore size distributions, compressive strength development in comparison with the reference portland cement. In addition, the hardened blended cement pastes were examined for crystalline hydration products using X-ray diffraction (XRD) analysis and for the microstructural and elemental composition of hydration products using Field Emissions Scanning Electron Microscope (FE-SEM) and electron microprobe analyzer (EPMA), respectively.

2. Materials and methods

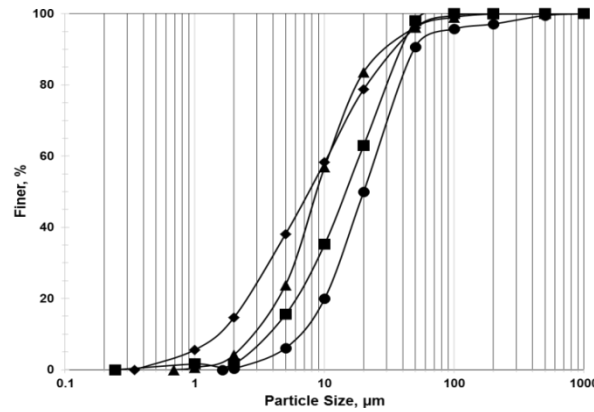


Fig. 1 Particle Size Distribution of Ordinary Portland Cement (OPC), coal fly ash (CFA), rice hull ash (RHA), sugar mill lime sludge (SMLS). Note: diamond: CFA; square: RHA; triangle: SMLS; circle: OPC

Table 1 Chemical composition of Ordinary Portland Cement (OPC), coal fly ash (CFA), rice hull ash (RHA) and sugar mill lime sludge (SMLS)

Elemental content, (%)	OPC	SMLS	RHA	CFA
SiO ₂	21.872	8.67	95.983	23.903
TiO ₂	0.288	0.031	0.026	0.592
Al ₂ O ₃	5.231	2.321	0.12	9.093
Fe ₂ O ₃	2.679	0.874	0.168	28.451
MnO	0.091	0.055	0.186	0.28
MgO	1.519	2.367	0.467	9.74
CaO	67.398	84.205	0.437	23.279
Na ₂ O	0.489	0.257	0.342	0.284
K ₂ O	0.481	0.296	1.107	0.582
P ₂ O ₅	0.227	0.156	0.534	0.062
SO ₃	2.146	0.667	0.016	2.966
Loss on Ignition (LOI)	3.0	46.10	9.231	15.997

2.1 Materials

Appropriate amounts of OPC, CFA, RHA and SMLS were collected and prepared prior to their utilization. Coal fly ash was collected from coal power plant at Villanueva, Misamis Oriental, Philippines, while the SMLS was collected from a sugar milling company at Butong, Quezon, Bukidnon, Philippines. In the case of RHA, rice hull samples were collected first from a local rice mill in Bukidnon, Philippines and were burned in a furnace at 700°C. The SCMs were prepared first by oven drying (if necessary) and followed by grinding using ball mill prior to blending. The particle size distributions of SCMs were measured using the particle size analyzer and is shown in Fig. 1. All the SCMs used were finer than OPC. The chemical composition of SCMs used in this study was analyzed by X-ray fluorescence (XRF). Table 1 summarizes the chemical composition

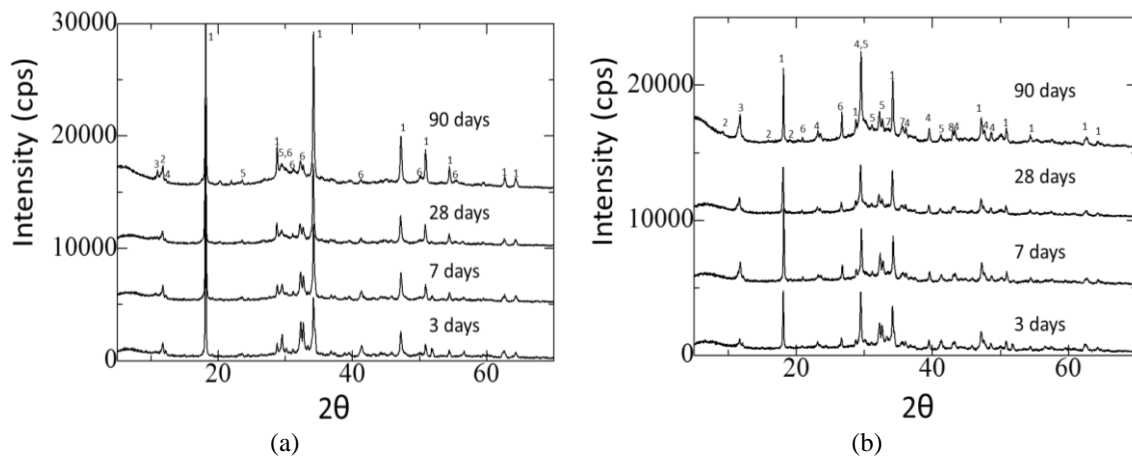


Fig. 3 XRD pattern of hydrated OPC (A) and hydrated blended OPC (B) at different curing days. Note: (A) - 1: Portlandite; 2: Monocarbonate; 3: Hemiacarbonate; 4: Ferrite; 5: Lime; 6: Alite (C_3S) & Belite (C_2S) (B) - 1: Portlandite; 2: Ettringite; 3: Monocarboaluminate; 4: Lime; 5: Alite (C_3S) & Belite (C_2S); 6: Quartz; 7: Hematite; 8: Brownmillerite

stopped by crushing the paste specimens into pieces of about 3-5 mm size. The samples were obtained by breaking the hardened cement paste. Representative samples were taken from the middle of the specimen and were immersed in isopropanol for 24 h. After that, the ground samples of hardened cement paste were freeze dried and placed in a vacuum desiccator prior to any analysis.

2.4 Experimental methods

2.4.1 XRD analysis

The mineralogical characterization of hardened cement pastes blended with SCMs and the reference material was examined at 3, 7, 28 and 90 days of curing age. The scanning range of 2θ were from 5 to 70° at 40 kV, 20 mA, step width 0.02° , and a scanning speed of $2^\circ/\text{min}$ and using a Cu α radiation X-ray diffractometer.

2.4.2 TG-DTA analysis

Thermo-gravimetric analysis was carried out for hardened cement pastes samples at different curing age. The sample was heated from room temperature to 1000°C at a heating rate of $10^\circ\text{C}/\text{min}$ under a nitrogen atmosphere. The thermogravimetric (TG) signal was used to calculate the weight loss during heating and to estimate the content of $\text{Ca}(\text{OH})_2$ (CH) and carbonated phases. The $\text{Ca}(\text{OH})_2$ content was calculated from the weight loss between 450 and 580°C .

2.4.3 Compressive strength determination of hardened cement paste

Three cubes were tested for each sample at the given curing age by using compression testing machine with 1000 kN capacity. Each strength value was an average of three specimens. Compressive strength of 25 mm cube specimens was determined at 3, 7, 28, and 90 days.

2.4.4 Microstructure of hardened cement paste

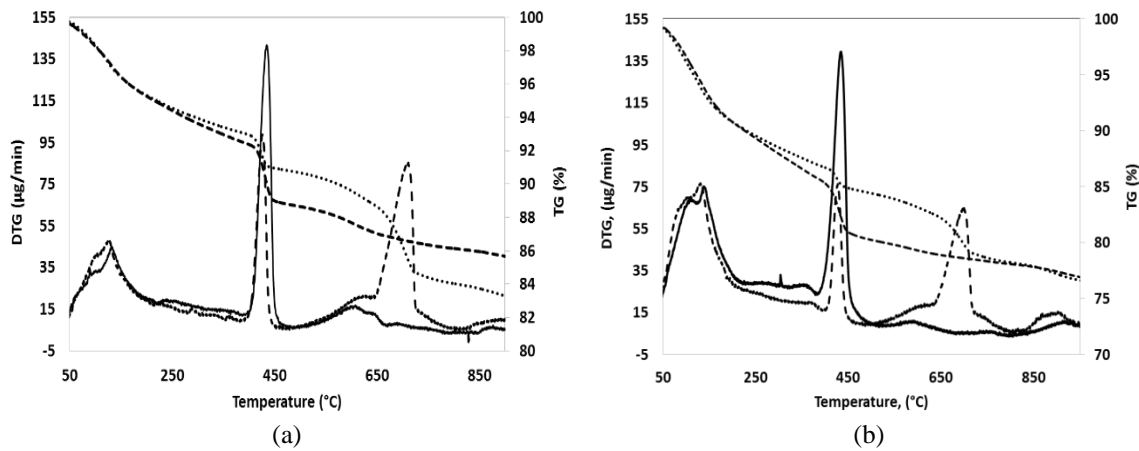


Fig. 4 TG-DTA pattern of hardened cement pastes after 3 (A) and 90 (B) days of curing. Note: Solid line: DTG-OPC; Dash line: DTG-Blended; Square dot: TG-OPC; Round dot: TG-Blended

Microstructure and hydration products of crushed hardened cement pastes were examined with scanning electron image (SEI). The SEI of the broken surface of the hardened cement was observed by field emission-scanning electron microscope (FE-SEM). The back scattered electron image (BEI) of the polished surface of hardened cement pastes and reference portland cement paste cured for 90 days was observed by electron probe microanalysis (EPMA). The pixel size was $20\ \mu\text{m}$ and the acceleration voltage was 15 kV with a counting interval of 50 ms. In addition, mercury intrusion porosimetry (MIP) was utilized to determine the pore size distribution of the hardened cement pastes cured for 3, 7, 28, and 90 days.

3. Results and discussion

3.1 XRD analysis hardened cement pastes

The peaks corresponding to CH with high intensities were observed as the major hydration products of hydrated OPC samples in the absence of SCMs as shown in Fig. 3. The CH intensity increases as the curing days progresses. Monocarbonate and hemicarbonate phases were also observed as hydration products in unblended samples. In contrast, the quaternary blended cement pastes showed lower CH intensities with only a slight increase in intensity after 90 days of curing. The significant reduction of CH intensity suggests that CH reacts with silica from RHA in which the pozzolanic action of RHA resulted in the formation of more CSH. The dilution effect could not be ruled out as well. In addition, ettringite and monocarboaluminate phases were observed as hydration products in cement pastes quaternary blended which could be attributed to CFA reaction. The variations of hydration product between the reference hardened OPC cement paste and blended OPC with SCMs were probably influenced by the balance between available alumina on one hand, and carbonate and sulfate on the other (Winter 2012). The presence of limestone for example leads to the formation of carboaluminate hydrates which was also reported in previous study by De Weerd *et al.* (2011). The presence of non-reactive crystalline phases of hematite and quartz in the hardened blended cement paste is attributed to CFA as source material.

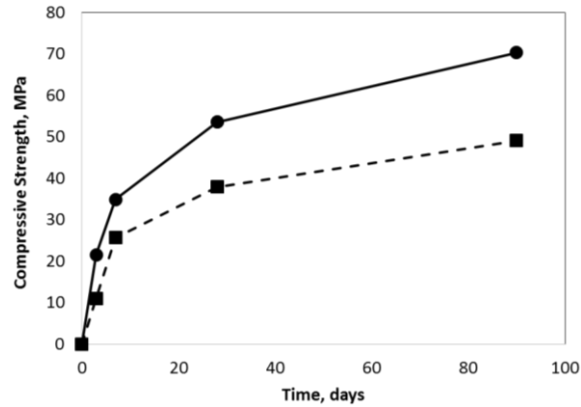


Fig. 5 Compressive strength of blended and plain hardened cement paste. Note: Round dot with solid line: Plain cement paste; Square dot with dash line: Blended cement paste

3.2 Thermogravimetric analysis

Fig. 4 shows the TG-DTA pattern of hardened cement pastes after 3 (A) and 90 (B) days of curing. Three step mass loss transitions can be observed clearly in hardened cement pastes blended with SCMs compared to plain cement paste. The mass loss at 105-450°C could be attributed to the dehydration of ettringite, CSH and calcium aluminate silicate hydrates (CASH). The second step mass loss between 450 and 580°C corresponds to the dehydration of $\text{Ca}(\text{OH})_2$ while the third step at 580 and 1000°C showed the mass loss of calcium carbonate (CaCO_3) (Kroehong *et al.* 2011). The peak in the DTG pattern corresponding to CH dehydration of blended cement pastes showed a significant decrease from 95 ug/min after 3 days of curing to 75 ug/min after 90 days of curing. The decrease in CH could indicate a change in the nature of the hydration products formed which was confirmed in the XRD pattern and similar to the reported results of De Weerd *et al.* (2011). Mass loss of ettringite, CSH and CASH, which were produced from OPC and even RHA, also created a peak on the DTG graphs of both plain OPC and blended samples. Also, the DTG peak corresponding to the mass loss of calcium carbonate was highly prominent in blended samples which could be attributed to lime sludge addition. The presence of calcium hydroxide ($\text{Ca}(\text{OH})_2$), which could have been produced from interactions with lime, CFA, and OPC, was visible in the blended samples although it is higher in plain OPC samples.

3.3 Compressive strength

Fig. 5 presents the compressive strength of hardened cement paste with and without SCMs under different curing days. The compressive strength of quaternary blended and plain cement paste increased with increasing curing period from 3 to 90 days and ranged from 11-49 MPa and 22-70 MPa, respectively. Although the compressive strengths at different curing periods of hardened cement paste blended with SCMs were lower compared to unblended samples, the percentage compressive strength of blended samples with the plain cement paste increased from 50% at 3 days to 70% after 90 days of curing period. The lower compressive strength of SCM blended cement paste may be attributed mainly to dilution effect caused by higher replacement of OPC with SCMs and the slow pozzolanic reactivity of the SCMs (De Weerd *et al.* 2011) coupled

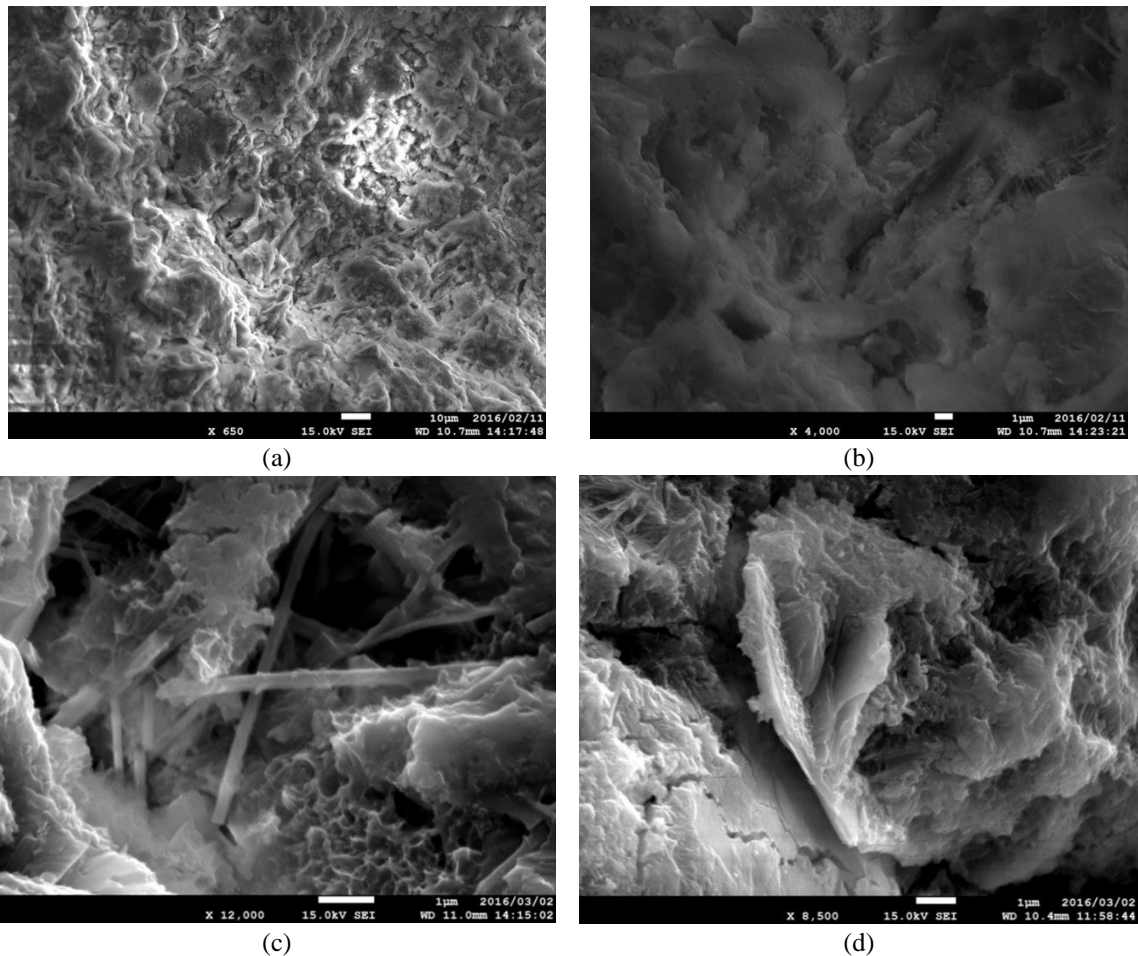


Fig. 6 FE-SEM images of hardened cement paste microstructure without SCMs after 3 days (a) and (b); and 90 days (c) and (d) of curing

with a higher water to cementitious ratio of 0.5. The filler effect of the SCMs used is not significant in increasing the compressive strength for higher water to cementitious ratio of greater than or equal to 0.5 (Wang 2017). The water-cement ratio highly affects the compressive strength due to its relationship with the amount of residual space i.e., capillary porosity, in the cement paste. Thus, adding more water leads to a more diluted cement paste that is weaker and vulnerable to cracks (Wong and Buenfeld 2009). However, the consideration of lower water to cementitious ratio which is a more rational option is beyond the scope of this study.

3.4 Microstructure of hardened cement pastes

3.4.1 FE-SEM observations

FE-SEM images of hardened cement paste with and without blended SCMs were taken after 3 and 90 days of curing are shown in Figs. 6 and 7. After 3 days of hydration, the plain cement pastes exhibited the general microstructural morphology of hardened cement paste. Extensive CSH

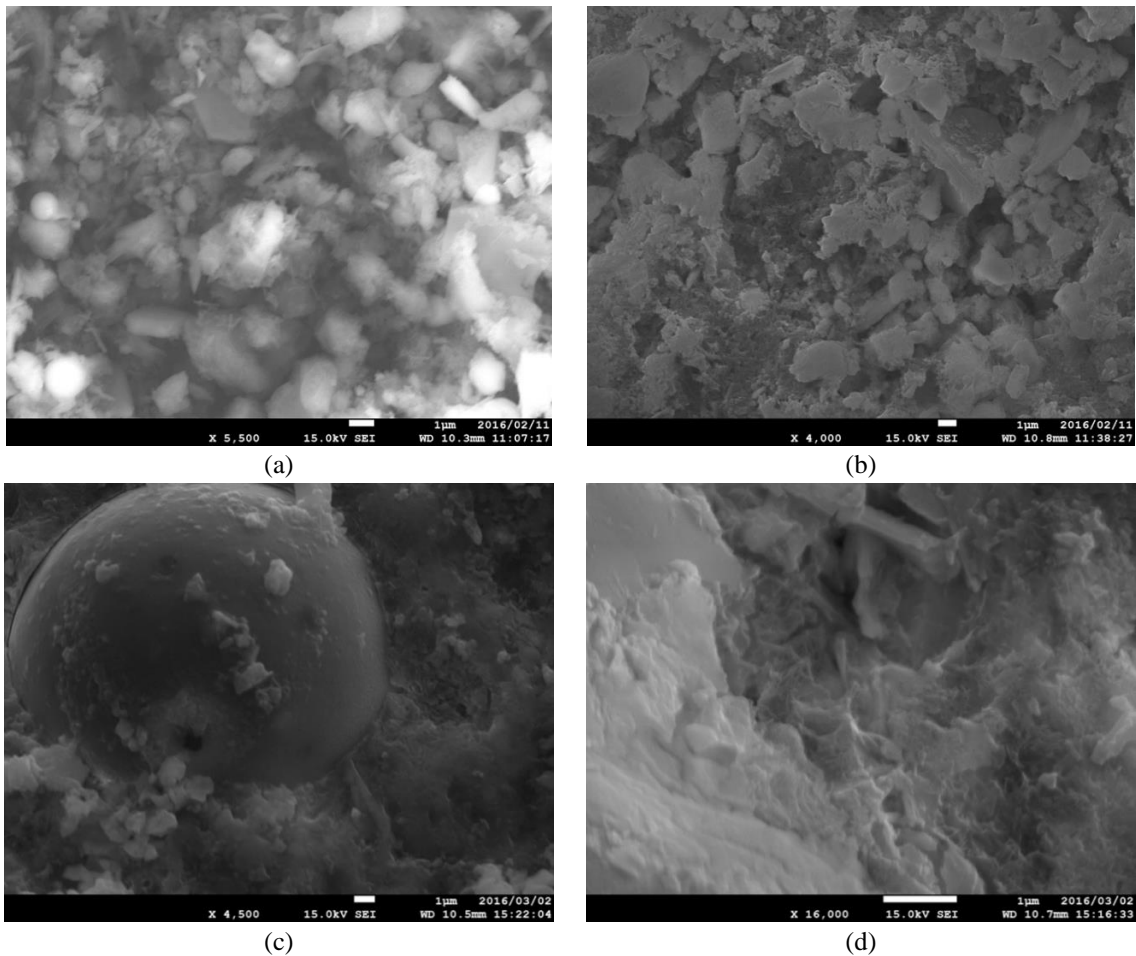
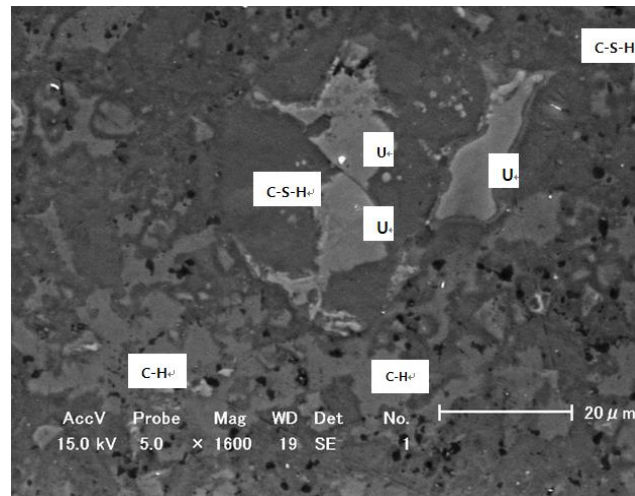


Fig. 7 FE-SEM images of the quaternary blended cement paste microstructure after 3 days (a) and (b); and 90 days (c) and (d) of curing

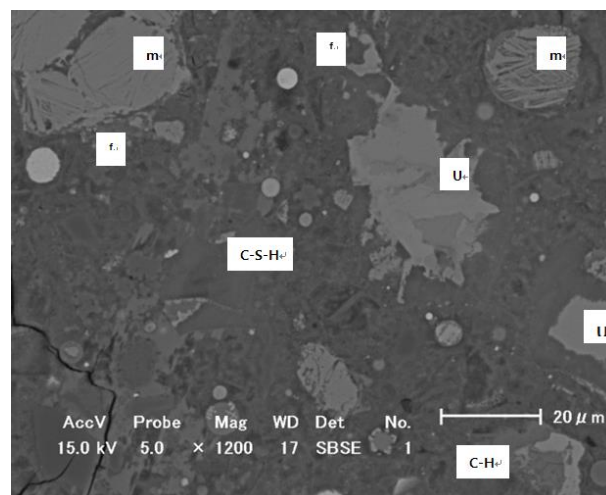
growth and ettringite needles were visible in addition to large portlandite crystals. The CSH network was more well-defined after 90 days while the ettringite and portlandite crystals were more evident. In contrast, the blended cement pastes after 3 days of curing showed unhydrated to partially hydrated SCMs grains and gel-like structures around the cement grains. These findings indicate a slow hydration process in SCM blended cement paste compared to plain cement paste. After 90 days of hydration, the blended cement paste already showed extensive CSH, CASH and portlandite growth but not well refined compared to plain cement paste. Also, gel-like structures around the CFA grain can be clearly seen including an area in which an active hydration process can be observed. This result suggests the slow reactivity of coal fly ash commonly reported in previous study of Hanehara *et al.* (2001). Calcium silicate hydrates particles can be observed also to fill the empty space in interfacial transition zone of cement paste that exists between cement grain and CFA particle.

On the other hand, the BEIs of polished surface of hardened plain cement paste (A) and blended cement paste (B) cured for 90 days are shown in Fig. 8. The brighter colored images



(a)

Fig. 8(a) BEI of polished surface of hardened plain cement paste (A) after 90 days of curing. Note: C-H: Ca(OH)₂; C-S-H: Calcium silicate hydrate; U: unhydrated cement



(b)

Fig. 8(b) BEI of polished surface of blended hardened cement paste (B) after 90 days of curing. Note: C-H: Ca(OH)₂; C-S-H: Calcium silicate hydrate; f: coal fly ash; U: unhydrated cement; m: AFm phases

could correspond to unhydrated cement grain. Partially hydrated cement paste surrounding an unhydrated core can also be observed. The relatively darker color relates to hydration products that may correspond to CSH and AFm phases. On the other hand, the blended cement paste showed many fly ash particles with clear borders. Calcium silicate hydrates and CASH phases were also evident but the microstructure was less dense compared to plain cement paste. Generally, the reaction of most SCMs is slower and difficult to follow as many SCMs consist of amorphous materials (Lothenbach *et al.* 2011).

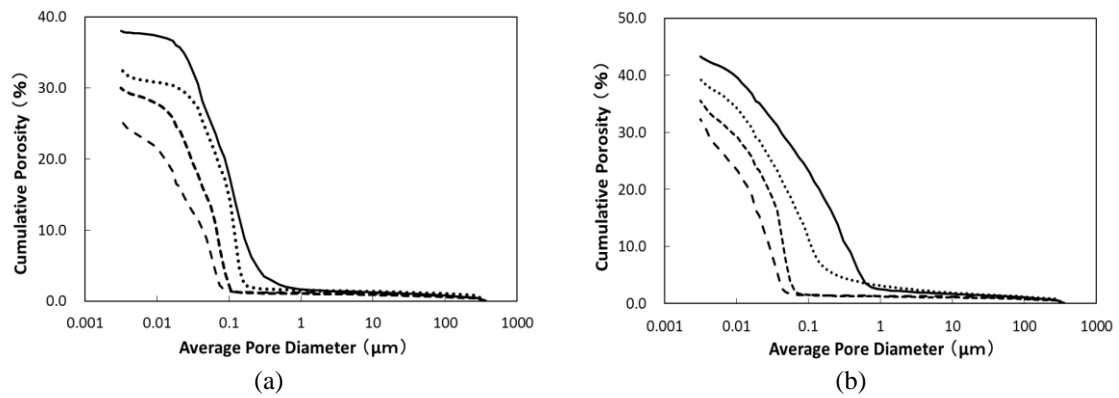


Fig. 9 Pore size distribution of plain (A) and blended (B) hardened cement paste. Note: Solid line: 3 days; Round dot: 7 days; Square dot: 28 days; Dash line: 90 days

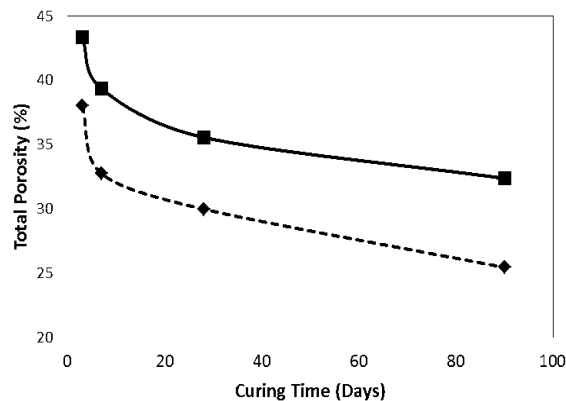


Fig. 10 Variation of total porosity of Control and Blended sample with curing days. Note: Square dot with solid line: Blended cement paste; Diamond dot with dash line: Plain cement paste

3.4.2 Pore size distribution

Fig. 9 shows the MIP curves of the plain portland (A) and blended (B) cement paste up to 90 days of curing. The pore volume intruded by mercury both decrease with curing time as the hydrates fill the pores. The measured pore distribution ranged from gel micropores (<4.5 nm), mesopores (4.5-50 nm), middle capillary pores (50-100 nm) and to large capillary pores (>100 nm) (Zeng *et al.* 2012). The pore volume decreases rapidly within the first 7 days and then decreases more slowly as shown Fig. 10. The results showed that incorporation of RHA, CFA SMLS in a quaternary blended cement pastes increased the total porosity and capillary porosity at all ages as compared to that of OPC paste. These results were similar to the findings of Berodier and Scrivener (2015) using slag and fly ash in ternary blended system with OPC which showed lower degree of reaction for high replacement levels of SCMs with constant water/cementitious material ratio. The lower degree of reaction could be attributed to the lack of water-filled capillary pores. Generally, at early age, the blended cement paste has a higher total porosity than plain OPC paste due to low clinker content and slow reaction of the SCMs (Pandey and Sharma 2000, Berodier and Scrivener 2015). CFA could also retard the hydration of C_3A and that of C_3S at early stages (Ramezani-pour 2014). On the other hand, higher water to cementitious ratio of 0.5 for cement

paste blended with higher replacements of SCMs could lead to higher space available. This could result to a limited reaction in the later stage due to the lack of water-filled capillary pores (Berodier and Scrivener 2015). Moreover, the high iron content in the fly ash used could have a deleterious effect on its pozzolanic activity. Mostly in fly ashes, iron oxide (Fe_2O_3) are present as nonreactive hematite and magnetite. It has to be separated from silica and alumina when chemical requirements and pozzolanic activity of fly ashes are considered (Ramezaniapour 2014).

4. Conclusions

Based on the experimental results, the synergistic reaction of CFA, RHA and SMLS with OPC in higher replacement percentage resulted to the formation of ettringite and monocarboaluminate and reduction of CH intensities compared to plain OPC. However, the microstructure of quaternary blended cement paste was less dense and exhibited higher total and capillary porosity at all ages compared to plain cement paste which resulted to a lower compressive strength of blended cement paste. The effect of higher water to cementitious ratio and lower degree of reaction of SCMs in higher replacement level hindered the positive effect of the synergistic reaction of SCM's used. Thus, these observations give additional insights on the determination of a rational option of water to cementitious ratio and the quality of SCMs to be selected in multi-blended systems to promote synergistic reaction. Good quality SCMs can become limited in the future as the demand increases in the utilization of blended cements.

Acknowledgments

This paper is an outcome of the first author's postdoctoral research fellowship at Hokkaido University, Sapporo, Japan. The authors acknowledge the financial support from DOST-PCIEERD through its BCDA postdoctoral research fellowship grant and Laboratory of Environmental Geology, Division of Sustainable Resources Engineering, Faculty of Engineering, Hokkaido University as host institution. The authors would like to thank also Dr. Kiyofumi Kurumisawa, Dr. Jun-ichi Kodama, Dr. Yoshiaki Fujii, Dr. Carlito Tabelin and Yu Arai for their support and helpful discussions.

References

- Berodier, E. and Scrivener, K. (2015), "Evolution of pore structure in blended systems", *Cement Concrete Res.*, **73**, 25-35.
- Chindaprasirt, P. and Rukzon, S. (2008), "Strength, porosity and corrosion resistance of ternary blend", *Constr. Build. Mater.*, **22**(8), 1601-1606.
- Chore, H.S. and Joshi, M.P. (2015), "Strength evaluation of concrete with fly ash and GGBFS as cement replacing materials", *Adv. Concrete Constr.*, **3**(3), 223-236.
- De Weerd, K., Kjellsen, K., Sellevold, E. and Justnes, H. (2011), "Synergy between fly ash and limestone powder in ternary cements", *Cement Concrete Compos.*, **33**(1), 30-38.
- Ferraro, R. and Nanni, A. (2012), "Effect of off-white rice husk ash on strength, porosity, conductivity and corrosion resistance of white concrete", *Cement Concrete Res.*, **31**, 220-225.
- Hanehara, S., Tomosawa, F., Kobayakawa, M. and Hwang, K. (2001), "Effects of water/powder ratio,

- mixing ratio of fly ash, and curing temperature on pozzolanic reaction of fly ash in cement paste”, *Cement Concrete Res.*, **31**(1), 31-39.
- Juenger, M.C. and Siddique, R. (2015), “Recent advances in understanding the role of supplementary”, *Cement Concrete Res.*, **78**, 71-80.
- Kathirvel, P., Saraswathy, V., Karthik, S.P. and Sekar, A.S. (2013), “Strength and durability properties of quaternary cement concrete made with fly ash, rice husk ash and limestone powder”, *Arab. J. Sci. Eng.*, **38**(3), 589-598.
- Kroehong, W., Sinsiri, T., Jaturapitakkul, C. and Chindaprasirt, P. (2011), “Effect of palm oil fuel ash fineness on the microstructure of blended cement paste”, *Constr. Build. Mater.*, **25**(11), 4095-4104.
- Lothenbach, B., Scrivener, K. and Hooton, R. (2011), “Supplementary cementitious materials”, *Cement Concrete Res.*, **41**(12), 1244-1256.
- Madandoust, R., Ranjbar, M., Moghadam, H. and Mousavi, S. (2011), “Mechanical properties and durability assessment of rice husk ash concrete”, *Biosyst. Eng.*, **110**(2), 144-152.
- Menendez, G. and Bonavetti, V. (2003), “Strength development of ternary blended cement with limestone filler”, *Cement Concrete Compos.*, **25**(1), 61-67.
- Nadeem, A., Memon, S.A. and Lo, T. (2013), “Mechanical performance, durability, qualitative”, *Constr. Build. Mater.*, **38**, 338-347.
- Panda, K.C. and Prusty, S.D. (2015), “Influence of silpozz and rice husk ash on enhancement of concrete strength”, *Adv. Concrete Constr.*, **3**(3), 203-221.
- Pandey, S.P. and Sharma, R.L. (2000), “The influence of mineral additives on the strength and porosity of OPC mortar”, *Cement Concrete Res.*, **30**, 19-23.
- Ramezaniapour, A. (2014), *Cement Replacement Materials*, Springer-Verlag Berlin Heidelberg, New Delhi, India.
- Wang, X.Y. (2017), “Modeling of hydration, compressive strength, and carbonation of portland-limestone cement (plc) concrete”, *Mater.*, **10**(2), 115.
- Winter, N.B. (2012), *The Fast Star User-friendly Insight into Cement Production, Cement Hydration and Cement and Concrete Chemistry*, WHD Microanalysis Consultants Ltd., U.K.
- Wong, H.S. and Buenfeld, N.R. (2009), “Determining the water-cement ratio, cement content, water content and degree of hydration of hardened cement paste: Method development and validation on paste samples”, *Cement Concrete Res.*, **39**(10), 957-965.
- Zeng, Q., Li, K., Fen-Chong, T. and Dangla, P. (2012), “Pore structure characterization of cement pastes blended with high-volume fly-ash”, *Cement Concrete Res.*, **42**(1), 194-204.